Journal of Anatomy

J. Anat. (2013) **223**, pp22–37 doi: 10.1111/joa.12053

Regrowth of transected retinal ganglion cell axons despite persistent astrogliosis in the lizard (*Gallotia galloti*)

María del Mar Romero-Alemán,[1] Maximina Monzón-Mayor,[1] Elena Santos[1,2] and Carmen M. Yanes[2]

[1]*Departamento de Morfología (Biología Celular), Universidad de Las Palmas de Gran Canaria, Canary Islands, Spain*
[2]*Departamento de Microbiología y Biología Celular, Universidad de La Laguna, Canary Islands, Spain*

Abstract

We analysed the astroglia response that is concurrent with spontaneous axonal regrowth after optic nerve (ON) transection in the lizard *Gallotia galloti*. At different post-lesional time points (0.5, 1, 3, 6, 9 and 12 months) we used conventional electron microscopy and specific markers for astrocytes [glial fibrillary acidic protein (GFAP), vimentin (Vim), sex-determining region Y-box-9 (Sox9), paired box-2 (Pax2), cluster differentiation-44 (CD44)] and for proliferating cells (PCNA). The experimental retina showed a limited glial response since the increase of gliofilaments was not significant when compared with controls, and proliferating cells were undetectable. Conversely, $PCNA^+$ cells populated the regenerating ON, optic tract (OTr) and ventricular wall of both the hypothalamus and optic tectum (OT). Subpopulations of these $PCNA^+$ cells were identified as $GFAP^+$ and Vim^+ reactive astrocytes and radial glia. Reactive astrocytes up-regulated Vim at 1 month post-lesion, and both Vim and GFAP at 12 months post-lesion in the ON-OTr, indicating long-term astrogliosis. They also expressed Pax2, Sox9 and CD44 in the ON, and Sox9 in the OTr. Concomitantly, persistent tissue cavities and disorganised regrowing fibre bundles reaching the OT were observed. Our ultrastructural data confirm abundant gliofilaments in reactive astrocytes joined by desmosomes. Remarkably, they also accumulated myelin debris and lipid droplets until late stages, indicating their participation in myelin removal. These data suggest that persistent mammalian-like astrogliosis in the adult lizard ON contributes to a permissive structural scaffold for long-term axonal regeneration and provides a useful model to study the molecular mechanisms involved in these beneficial neuron–glia interactions.

Key words: axonal regeneration; long-term gliosis; reptile; retino-tectal system.

Introduction

To date, the snake *Vipera aspis*, and lizards *Ctenophorus ornatus* and *Gallotia galloti* are the only amniotes capable of successful axonal regrowth after optic nerve crush or transection (Rio et al. 1989; Beazley et al. 1997; Lang et al. 1998; Dunlop et al. 2000). These two axotomy methods offer complementary views of spontaneous central nervous system (CNS) axonal regeneration capacity *in vivo*. The meningeal sheath remains intact as a conduit for regeneration in crush lesions, which better mimics the CNS environment, e.g. the inflammatory response is more limited and severed axons remain more closely adjacent to each other, as do proximal (or rostral) and distal (or caudal) nerve stumps. However, the severity of transection injury is greater and imitates the most harmful CNS traumatic injuries in mammals. This proves a bigger challenge for retinal ganglion cells (RGCs) to survive and to regenerate axons. Accordingly, differences in the time course of RGC axonal regeneration between these lizard species seem to be linked to the chosen injury model (Table 1) and not to intrinsic species-specific properties. In fact, the horseradish peroxidase (HRP) tracing experiments in *G. galloti* revealed that severed axons cross over the transection site after 2 months (Lang et al. 2002) and the crush site after only 3 weeks (Dobson, 2010), which is similar in timing (1 month) to that observed at the crush site of *C. ornatus* (Dunlop et al. 2000). Interestingly, the RGC survival capacity in both lizard species was similar (around 70%) despite the fact that transected RGC axons in *G. galloti* took 6–9 months to reach the optic tectum, which is a considerable delay when compared with the 2 months that crushed axons took in *C. ornatus* (Lang et al. 2002; Dunlop et al. 2004; Santos,

Correspondence
Dr María del Mar Romero-Alemán, Departamento de Morfología (Biología Celular), Facultad de Ciencias de la Salud, Universidad de Las Palmas de Gran Canaria, Plaza Dr. Pasteur s/n., 35016 Las Palmas, Canary Islands, Spain. T: + 34 928 453425; F: + 34 928 453420; E: mromero@dmor.ulpgc.es

Accepted for publication *1 April 2013*
Article published online *8 May 2013*

© 2013 Anatomical Society

Table 1 Summary of comparative RGC axon regeneration process between lizard species.

	Lizard *G. galloti*	Lizard *C. ornatus*	References
Continuous retinal proliferation and neurogenesis	Absent	Absent	Beazley et al. (1998); Casañas et al. (2011); Lang et al. (2002)
RGC axon projection in control conditions	Entirely towards the contralateral optic tectum		Dunlop et al. (2004, 2007); Lang et al. (2002)
Predominant injury model	Optic nerve transection (ONT)	Optic nerve crush (ONC)	Beazley et al. (1997); Lang et al. (1998)
RGC survival	Around 70% (12 m.p., ONT)	Around 70% (12 m.p., ONC) 100% (12 m.p., incomplete ONC)	Beazley et al. (1997); Dunlop et al. (2007); Santos (2008)
RGC axons cross over the lesion site	By 3 weeks (ONC) By 2 months (ONT)	By 1 month (ONC)	Dobson, 2010; Dunlop et al. (2000); Lang et al. (2002)
Misrouting axons towards the ipsilateral optic tract	Detected (HRP tracing, ONT)	Detected (DiI tracing, ONC)	Dunlop et al. (2004, 2007); Lang et al. (2002)
Misrouting axons towards the intact optic nerve	Undetected (HRP tracing, ONT)	Undetected (DiI tracing, incomplete ONC)	
RGC axons reach the contralateral optic tectum	By 6–9 m.p. (ONT)	Between 1–2 m.p. (ONC)	Dunlop et al. (2004); Lang et al. (2002)
Recovery of the retinotopic order in the optic tectum	No data	Failed (ONC) Restored (incomplete ONC)	Beazley et al. (1997); Dunlop et al. (2007)
Functional regeneration	Minimal (recovery of pupillary light reflex, ONT)	Partial (after ONC + visual training) Restored (incomplete ONC)	Beazley et al. (2003); Dunlop et al. (2007); Yanes et al. (2011)
Up-regulation of axonal growth inhibitors	Detected (IN1, Nogo-A, Tenascin-R, CSPG)	No data	Dobson (2010); Lang et al. (1998, 2008)
Up-regulation of axonal growth promoters	Detected (laminin, fibronectin, BDNF, NT-3)	Detected (PSA-NCAM, GAP-43)	Harman et al. (2003); Lang et al. (2008); Rodger et al. (2001); Santos et al. (2008, 2011)

m.p., months post-lesion; RGC, retinal ganglion cell.

2008). In addition, the regrowth of transected RGC axons in *G. galloti* occurred in a putative non-supportive microenvironment represented by persistent GFAP$^+$ astrogliosis (Lang et al. 2002, 2008), up-regulation of axonal growth inhibitors (Lang et al. 1998, 2008; Dobson, 2010) and absence of continuous retinal proliferation and neurogenesis (Lang et al. 2002; Casañas et al. 2011). In contrast, the optic nerve regeneration in anamniotes (e.g. fish and frogs) occurs in a highly supportive microenvironment characterised by transitory gliosis (Stafford et al. 1990), lack or down-regulation of axonal growth inhibitors (Becker et al. 1999, 2004), adult retinal neurogenesis, up-regulation of axonal growth promoters (Caminos et al. 1999; Schweitzer et al. 2003) and participation of invading Schwann cells in the promotion of axon regrowth and remyelination (e.g. fish, Nona et al. 2000). These differences may account for the complete restoration of the visual function in fish and amphibians as compared with the limited functional recovery in *C. ornatus* (Beazley et al. 2003) and *G. galloti* (Yanes et al. 2011).

Reactive gliosis, mainly involving reactive astrocytes, is observed after different kinds of injury and neurodegenerative processes in the CNS of adult vertebrates. Reactive astrogliosis is characterised by cellular hypertrophy, hyperplasia, migration, and an increased expression of certain proteins such as glial fibrillary acidic protein (GFAP), vimentin (Vim), nestin (review in Robel et al. 2011) and glutamine synthetase (GS) (Benton et al. 2000). In acute CNS injury in mammals, reactive astrocytes may initially be protective to repair the blood–brain barrier, prevent an overwhelming inflammatory response and limit cellular degeneration (review in Robel et al. 2011). However, the long-lasting astroglial scar prevents axonal regrowth through the formation of a physical barrier and the secretion of axonal growth inhibitory molecules, such as chondroitin sulphate proteoglycan (CSPG) in the extracellular matrix (review in Busch & Silver, 2007). Accordingly, transitory reactive astrogliosis is observed during the successful optic nerve regeneration of anamniotes (Stafford et al. 1990; Nona, 2005) and after stab wound injury in the cerebral cortex of the amniote *G. galloti* (Romero-Alemán et al. 2004). Strikingly, our preliminary data reveal persistent GFAP$^+$ astrogliosis and up-regulation of putative axonal

© 2013 Anatomical Society

growth inhibitors (e.g. Tenascin-R, CSPGs, Nogo-A) in the regenerating lizard visual system (Lang et al. 2002, 2008; Dobson, 2010). Moreover, these reactive astrocytes apparently do not increase glutamine synthetase (GS) and vesicular glutamate transporter-1 (VGLUT1) (Romero-Alemán et al. 2010).

By taking into account the importance of the glial response for the regenerative capacity of the CNS, the intermediate phylogenetic position of reptiles between regeneration-competent (e.g. amphibians) and -deficient vertebrates (e.g. birds and mammals), and lack of data in reptiles, we previously immunocharacterised astroglial cells in the developing and adult lizard visual system (Monzón-Mayor et al. 1990a,c; Romero-Alemán et al. 2010, 2012; Casañas et al. 2011). The present study focuses on a more profound immunocharacterisation and analysis of reactive astrogliosis in the lizard visual system in order to complete our previous data and to compare them with those obtained in regeneration-competent and -deficient species. We analysed the reactive changes of Müller glia, astrocytes and radial glia after optic nerve transection in relation to the expression of the proliferating cell nuclear antigen (PCNA) and astroglial markers Vim, GFAP, adhesion molecule cluster differentiation 44 (CD44), the transcription factors paired box 2 (Pax2) and sex-determining region Y-box 9 (Sox9), as well as using conventional electron microscopy. The quantification of the changes in Vim and GFAP immunolabelling was performed to check the statistical significance of the apparent increase in these gliofilaments during the time course of astrogliosis. Although CD44, Sox9 and Pax2 have not been seen to be typical markers of astrogliosis, they are expressed by the astroglial lineage of the vertebrate visual system (Ries et al. 2007; Casañas et al. 2011; Romero-Alemán et al. 2012). Moreover, reactive astrocytes have been reported to increase CD44 and Sox9 after spinal cord injury in rats (Moon et al. 2004; Gris et al. 2007) and to up-regulate both Pax2 mRNA in mouse retina *in vitro* (Dharmarajan et al. 2012) and Sox9 around human cerebellum tumours (Kordes & Hagel, 2006). Therefore, we believed it would be of interest to analyse the response of these markers in *G. galloti*. The insight gained could be relevant for not only a comparative view of the permissive microenvironments supporting the axonal regeneration process, but also for proposing a mammalian-like model of long-term astrogliosis linked to successful axonal regeneration and to depict the scenario of glial permissiveness in amniotes.

Materials and methods

Animal maintenance and surgical procedure

We used 36 adult *G. galloti* lizards, which are indigenous to the Canary Islands (Spain). They were collected in their natural environment in compliance with local legislation, and were maintained and treated in the laboratory according to Spanish and European animal welfare legislation. Lizards had daily cycles of 12 h light/dark, free access to water and a mixed diet of commercial cat food and fresh fruits. The temperature in the holding tanks was maintained at around 25 °C, similar to their natural environment. Unilateral optic nerve transection was performed according to Romero-Alemán et al. (2010). Briefly, adult lizards were anaesthetised by intraperitoneal injection with diazepam 12.5 mg kg^{-1} and ketamine 250 mg kg^{-1}. An incision was made in the supraocular osteodermal plaque to expose the optic nerve, which was transected about 1 mm from the eye using iridectomy scissors. Next, the osteodermal plaque was put back into place. Lizards recovered and behaved normally. The post-lesion time points for this study were selected in accordance with our previous studies on this species (Lang et al. 2002, 2008; Romero-Alemán et al. 2010). Thus, lesioned animals were allowed to recover over periods of 0.5, 1, 3, 6, 9 and 12 months. At least three animals were examined at each time point by comparing the experimental side with the contralateral one, and with non-lesioned control animals.

Primary antibodies

The primary antibodies used in this study were previously characterised and recognised for a specific protein band in lizard brain extracts (Romero-Alemán et al. 2010, 2012; Casañas et al. 2011; Santos et al. 2011) in accordance with their predicted molecular weight in other species. This indicates an interspecies conservation of the corresponding epitopes. Immunofluorescence and immunoperoxidase detection was done using the following mouse monoclonal antibodies: anti-PCNA (1 : 60, cat # P8825, clone PC10; Sigma-Aldrich, St. Louis, MO, USA), anti-Vim (1 : 100, cat # H5, Developmental Studies Hybridoma Bank, Iowa City, IA, USA), anti-GFAP antibody (1 : 500, cat # G3893, clone GA5, Sigma-Aldrich), anti-phosphorylated neurofilament (1 : 1000, cat # SMI-31R, lot 17; Sternberger/Covance, Berkeley, CA, USA), anti-GS antibody (1 : 500, Cat # MAB302, lot LV1457801; Chemicon, Temecula, CA, USA); and the following rabbit polyclonal antibodies: anti-GFAP (1 : 100, cat # 4650-0204, lot 24042604; Biotrend Chemikalien GmbH, Cologne, Germany), anti-Pax2 (1 : 200, Cat # PRB276P0200; Covance, Berkeley, CA, USA), anti-Sox9 (1 : 2000, a kind gift of Dr Michael Wegner, Erlangen, Germany) (Stolt et al. 2003) and anti-CD44 (1 : 500, cat # ab65829; Abcam, Cambridge, UK).

Immunohistochemistry

Most immunostainings were obtained using Bouin's fixative and paraffin sections. However, optimal Sox9 staining required fixation with 4% paraformaldehyde and cryosections. Paraffin sections were dewaxed and hydrated, and antigen retrieval was then achieved by microwaving sections at full power (700 W) in 0.01 M citrate buffer, pH 6 for 10 min.

Double immunofluorescence labellings were performed for the simultaneous detection of the monoclonal and polyclonal markers. Sections were first pre-incubated in Tris buffered saline (TBS; 0.05 M Trizma base containing 150 mM of NaCl, pH 7.4) containing 1% bovine serum albumin (BSA) and 0.1% Tween-20 for 1 h at room temperature. Then they were incubated with the primary antibodies diluted in TBS-BSA overnight in a humid chamber at 4 °C. Afterwards, they were incubated with anti-mouse IgG Cy3 (1 : 1000, Jackson Immunoresearch, West Grove, PA, USA) and anti-rabbit Alexa Fluor 488 (1 : 1000, Molecular Probes, Eugene, OR, USA) for 1 h. Finally, sections were counterstained with 4′, 6-diamidino-2-

© 2013 Anatomical Society

phenylindole dihydrochloride (DAPI) nuclear dye for 10 min and mounted in Mowiol. All the slides were stored in the dark at 4 °C until examination.

For immunoperoxidase stainings, sections were immersed in a solution of 3% H_2O_2 in TBS to block endogenous peroxidase and were then pre-incubated in TBS-BSA for 1 h. Next, sections were incubated with the primary antibody, followed by incubation with a biotinylated anti-mouse IgG antibody or a biotinylated anti-rabbit IgG (1 : 500, Vector, Burlingame, CA, USA) for 1 h, and avidin-peroxidase (1 : 400, Sigma-Aldrich) for 1 h. Peroxidase activity was revealed with diaminobenzidine (DAB) solution. For the double immunoperoxidase stainings, the sequential detection of antigens consisted of revealing one of them in black/dark grey using DAB solution containing 1% ammonium nickel sulphate, whereas only DAB was used afterwards with the other one in brown. Finally, sections were washed three times in TBS to be dehydrated in ethanol series, cleared in xylene and mounted in Eukitt.

Negative controls consisted in omitting primary antibodies and replacing them with the corresponding non-immune serum. In addition, the negative controls for the mouse monoclonal antibodies also consisted in replacing them with the corresponding isotype control antibody. No immunostaining was detected in any of these negative controls, thus supporting the validity of the immunohistochemical results.

Quantification of vimentin and GFAP immunostaining intensity and statistical analysis

To detect whether apparent changes in the staining intensity of these gliofilaments were statistically significant in the regenerating process along the visual pathway, we compared the data obtained in the retina (central retina and its far peripheral edge), optic nerve (caudal nerve) and optic tract of control lizards with their counterparts in lesioned animals before the onset of axonal regrowth at the lesion site [1 month post-lesion (m.p.)] and after regrowing axons reached the optic tectum (12 m.p.). Staining intensity was quantified after acquiring sets of images obtained from sections of identical thicknesses with identical exposure times. Images were analysed with IMAGEJ 1.42 software (URL http//imagej.nih.gov/ij/docs/). Three animals per group ($n = 3$) and at least three sections per animal were used. Measurements of the same area were taken using a 40× objective in the region of interest per section. For each marker (vimentin, GFAP) and location (caudal nerve, optic tract, far peripheral retina), data were analysed according to the following mixed model (Laird & Ware, 1982): $Y_{i,time,\ lesion} = \theta + \beta_{time} + \gamma_{time,\ lesion} + a_i + e_{i,\ time,\ lesion}$ (time = Control, 1 m.p., 12 m.p.; lesion = yes, no) where Y is the marker, β_{time} is the period effect ($\beta_{Control} = 0$), $\gamma_{time,\ lesion}$ is the added effect of the lesion (hence, $\gamma_{time,\ no} = 0$), a_i is the effect of the i*th* animal and $e_{i,\ time,\ lesion}$ is the variability in the i*th* animal. The model was estimated by the method of maximum likelihood. Data are presented as means adjusted for the model (standard error). Multiple comparisons among the mean values measured in all the sections from each location were made using the corresponding *F*-test. The level of significance was set at $P < 0.05$. Data were analysed using the R-package (R Development Core Team, 2012).

Transmission electron microscopy

Three lesioned animals were examined at various time points (0.5, 1, 3 and 9 m.p.) for conventional electron microscopy in accordance with Santos et al. (2006). Briefly, animals were anaesthetised as previously reported and were perfused transcardially using 2.5% glutaraldehyde in 0.1 M Milloning buffer, pH 7.2. The retinas, optic nerves, optic tracts, optic chiasms and optic tecta were dissected and post-fixed in the same fixative for 4 h at 4 °C. After washing in Milloning buffer, tissue samples were immersed in 1% osmium tetroxide for 4 h at room temperature and were then dehydrated in graded acetone. Tissue samples were stained with 2% uranyl acetate in 70% ethanol overnight during the dehydration procedure and were finally embedded in Araldite. Semithin sections (1 μm thick) and ultrathin sections (80 nm thick) were stained with toluidine blue and lead citrate, respectively.

Image acquisition and processing

Photomicrographs were taken using a Zeiss Axiovert 200 M light microscope (Carl Zeiss, Göttingen, Germany) equipped with epifluorescence, an Axiocam HRm camera and a Canon Powershot A620 colour camera. Ultrathin sections were observed and captured using a Jeol 1010 (ULL, Jeol GmbH, Eching, Germany) or a Zeiss 910 (ULPGC, Carl Zeiss, Oberkochen, Germany) transmission electron microscope. Images were digitally processed using the AXIOVISION rel. 4.6 software and the Adobe PHOTOSHOP 6.0 software. Only general contrast adaptations were made and figures were not otherwise manipulated.

Results

The rostro-caudal axis is considered for orientation purposes. In the text, the term 'rostral optic nerve' refers to the portion between the eye and the lesion site, and the 'caudal optic nerve' refers to the portion between the lesion site and the optic chiasm.

The immunolabellings of astroglial markers are described along the lizard visual system from the retina to the optic tectum. The comparisons of the control (non-lesioned) and experimental animals were analysed. After unilateral optic nerve transection, all the immunohistochemical markers on the intact side of the visual pathway apparently showed similar staining patterns to those in the control animals. However, some significant differences were observed between the Vim and GFAP staining intensity values recorded in the control animals and on the intact side of the lesioned animals (Fig. 1F). Therefore, the intact side of the lesioned animals did not suffice as a valid reference of the control conditions and a comparison with the group of non-lesioned animals had to be made. The data were considered statistically significant for these two references. To prevent repetitive imaging, only the most relevant changes and time points are depicted in the figures.

Changes in the experimental retina

The labelling pattern for GFAP and Vim in the control retina showed a predominant Müller glia endfeet location (Fig. 2A,C). In the experimental retina, Vim and GFAP staining spread to the inner Müller glia processes and its branches (Fig. 2B,D). However, our statistical analyses on

© 2013 Anatomical Society

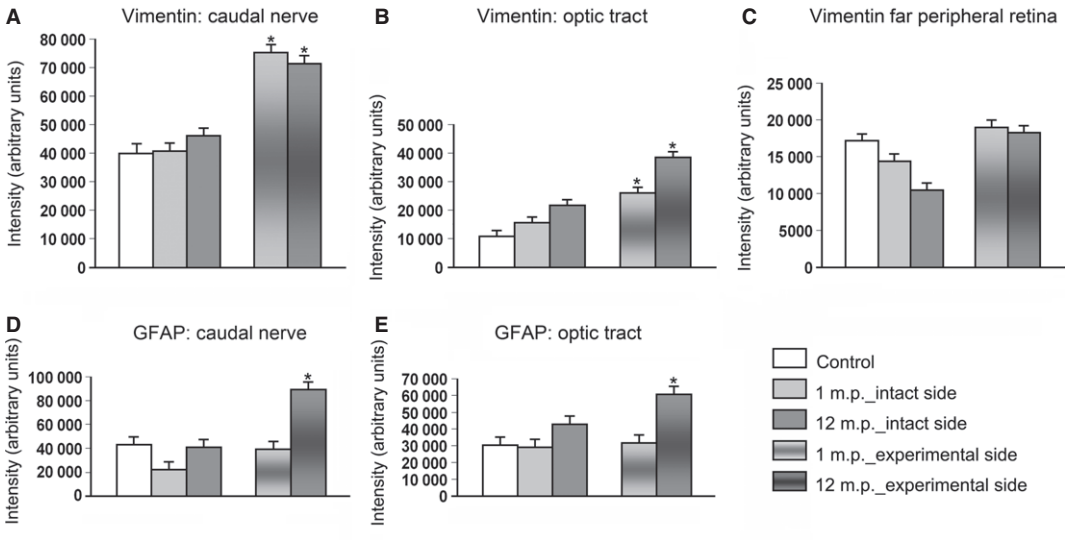

F

Marker	Location	Side	Control †	1 m.p.	12 m.p.
Vimentin	Caudal nerve	Intact	40 008 (2781) [a]	40 733 (2781) [a]	46 060 (2781) [a]
		Experimental		75 220 (2887) [b*]	71 304 (2887) [b*]
	Optic tract	Intact	10 721 (2001) [a]	15 402 (2001) [a]	21 572 (2001) [b]
		Experimental		25 853 (2001) [b*]	38 348 (2001) [c*]
	Far peripheral retina	Intact	17 155 (920) [a,c]	14 375 (969) [a]	10 422 (969) [b]
		Experimental		19 020 (969) [c]	18 260 (920) [c]
GFAP	Caudal nerve	Intact	42 978 (6496) [a]	21 846 (6616) [b]	40 791 (6616) [a]
		Experimental		39 102 (6616) [a]	89 415 (6496) [c*]
	Optic tract	Intact	30 393 (4717) [a]	28 965 (4857) [a]	42 838 (4857) [b]
		Experimental		31 596 (4857) [a]	60 533 (4867) [c*]

Fig. 1 Quantitative analysis of vimentin and GFAP immunostaining along the visual pathway of control lizards before the onset of axonal regrowth (1 m.p.) and after the regrowing axons reached the optic tectum (12 m.p.). (A-E) Bar graph representation of the mean values (± SEM) for vimentin and the GFAP measurements corresponding to the table of the numerical data in (F). The asterisks in the bar graphs and in the table (F) represent a significant increase of staining intensity in comparison with both controls and the contralateral sides. Densitometric measurements are represented as the values on an arbitrary scale provided by the image analysis software. Note that vimentin staining is up-regulated in the caudal nerve (A) and optic tract (B) at 1 and 12 m.p., whereas no significant increase is detected in the far peripheral retina in comparison with controls (C). GFAP immunolabelling is up-regulated in the caudal nerve (D) and optic tract (E) only at 12 m.p. (F) Data are the adjusted means (± SEM) by the mixed-models. (†) At each location, controls are common to both sides. The control group is compared with that at 1 m.p. and 12 m.p., and the two latter are also compared. Different superscript letters (^{a,b,c}) between sides/groups indicate statistical significance ($P < 0.05$, $n = 3$), whereas the same superscript letter denotes non-significance. Note that the superscript letter in the experimental side is usually different to that in the corresponding intact side, indicating statistical significance. However, the latter is not always a valid reference of the control conditions since there are some significant changes (different superscript letters) between the values recorded in the control animals and on the intact side of the lesioned animals. Thus, measurements in the control group are required as a baseline reference for valid statistical results.

GFAP in the central retina (not shown) and on Vim on its far peripheral edge revealed a non-significant increase after 1 and 12 m.p. in comparison with controls (Fig. 1C,F). At the different time points studied, PCNA immunolabelling was not detected in either the control (Fig. 2A,C) or the experimental retina (Fig. 2B,D). Moreover, transcription factors Sox9 (Fig. 2E–F′) and Pax2 (Fig. 2H,I) apparently remained unchanged in the Müller glia nuclei of the experimental retina. These glial cells were clearly identified by the coexpression of GS and Sox9 (inset in Fig. 2E). Under the control and experimental conditions, $Sox9^+$ Müller glia were detected along the entire retina, whereas $Pax2^+$ Müller glia predominated in the central retina. Moreover, the retina-optic nerve junction was delimited by rows of astroglial nuclei expressing both Pax2 (Fig. 2H,I) and Sox9 (Fig. 2G). Ultrastructurally, the Müller glia processes and endfeet in the experimental retina showed a developed smooth endoplasmic reticulum and abundant gliofilaments (Fig. 3A), and their processes remained joined by desmosomes (Fig. 3B). Branches of the inner processes of the Müller glia enwrapped the regenerating retinal ganglion cells (Fig. 3B) and large myelinated axons in the nerve fiber layer (Fig. 3C). These myelin sheaths showed loose, irregular profiles (inset in Fig. 3C), as in the control retina.

Immunocharacterisation and ultrastructure of the astrogliosis in the experimental optic nerve

Our statistical analysis revealed a significant increase in Vim, but not in GFAP, caudal to the lesion site (caudal optic

© 2013 Anatomical Society

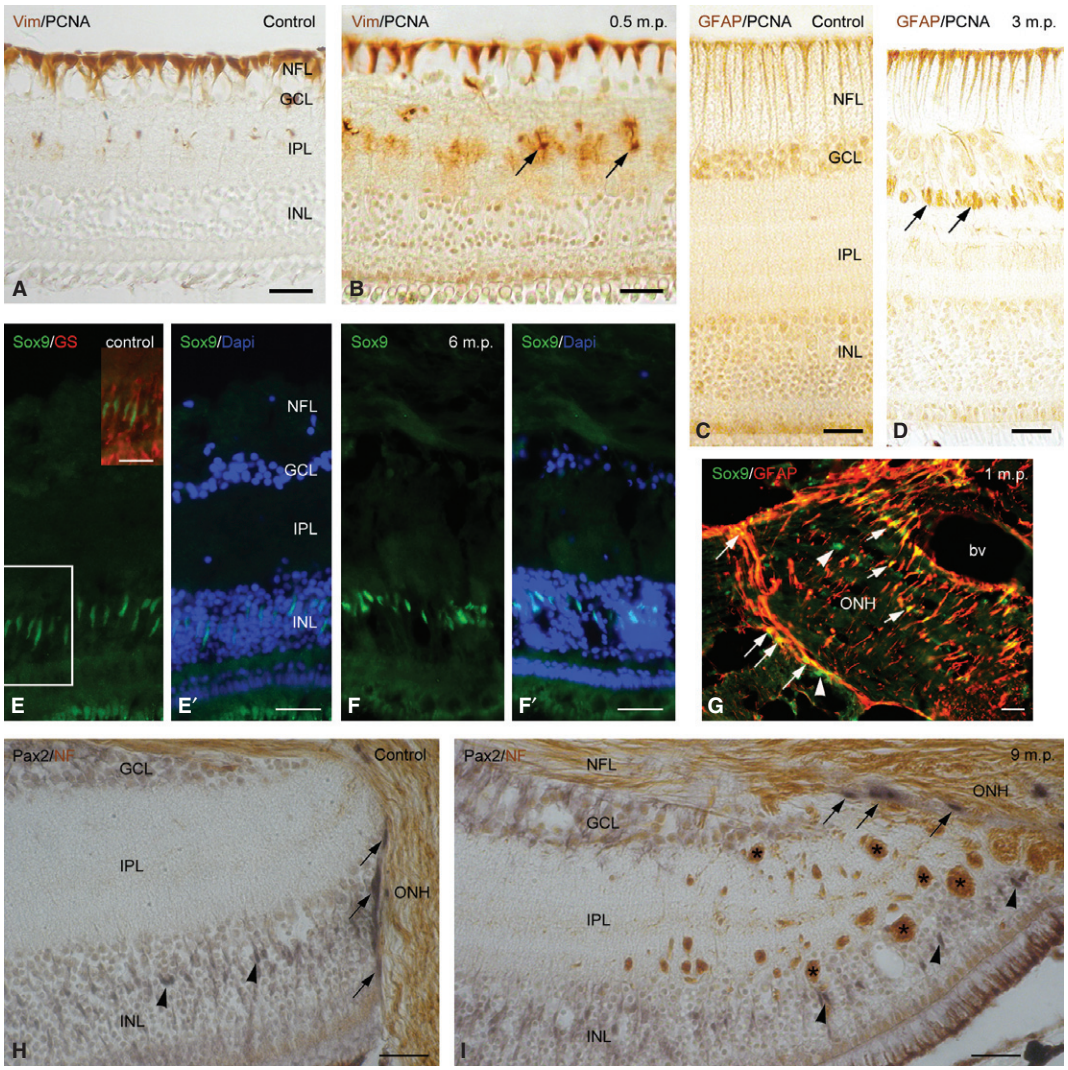

Fig. 2 Expression of the proliferating and astroglial markers in the control and experimental retina revealed by PCNA, Vim, GFAP, Sox9 and Pax2 immunolabelling. (A-D) Double immunoperoxidase staining for Vim/PCNA on the far peripheral edge of the control (A) and experimental retina at 0.5 m.p. (B), and for GFAP/PCNA in the central retina of the control (C) and experimental animals at 3 m.p. (D) Nomarski optic. Note that proliferating cells (black signal) are not detected in the retina of either the control or the experimental animals. In the control lizards, Müller glia endfeet are Vim^+ (brown signal in A) and $GFAP^+$ (brown signal in C). Under experimental conditions, Vim and GFAP spread to branches of the inner Müller glia processes located in the IPL (arrows in B) and GCL (arrows in D). (E-F′) Immunofluorescence labelling for Sox9 and Dapi counterstaining in the central retina of the control (E,E′) and experimental animals at 6 m.p. (F,F′). In the control retina, the $Sox9^+$ Müller glia nuclei are aligned in the midline of the INL (E) and coexpress GS (the inset in E corresponds to the boxed area). Note a similar staining pattern at 6 m.p. (F,F′). (G) Double immunostaining for Sox9 (green signal) and GFAP (red signal) at 1 m.p. $Sox9^+$ astrocytes coexpress GFAP along the retina-optic nerve junction (long arrows), and in the optic nerve head (ONH, short arrows) which shows a major blood vessel (bv) in its centre. Note the few $Sox9^+/GFAP^-$ astrocytes (arrowheads). (H,I) Double immunoperoxidase staining for Pax2 (in black) and phosphorylated neurofilaments (NF, in brown) in the central retina of controls (H) and at 9 m.p. (I) Nomarski optic. Note the $Pax2^+$ Müller glia nuclei in the middle of the INL (arrowheads in H and I) and the $Pax2^+$ astrocytes nuclei delimiting the retina-optic nerve junction (arrows in H and I). Misrouted NF^+ regenerating nerve fascicles are transversally cut in the experimental central retina (asterisks in I). For abbreviations, see text. Scale bars: 25 μm.

nerve and optic tract) at 1 m.p., whereas both Vim and GFAP immunolabelling increased significantly at 12 m.p. (Fig. 1A,B,D,E).

At 0.5, 1 and 3 m.p., reactive astrocytes were observed mainly on the borders of the lesion site (Fig. 4A–D). These hypertrophied astrocytes were $GFAP^+$ (Fig. 4A) and Vim^+ (Fig. 4B), and they coexpressed GFAP/Vim (not shown), GFAP/Sox9 (Fig. 4A inset) Vim/Sox9 (Fig. 4C), Vim/Pax2 (not shown) and GFAP/Pax2 (Fig. 4D), whereas putative invasive connective tissue and mesodermic cells (e.g. fibroblasts, macrophages) were unstained (asterisk in Fig. 4A–E). The proliferating cells expressing PCNA were not detected along the visual pathway of the control animals (not shown). In contrast, they were commonly stained in the experimental

© 2013 Anatomical Society

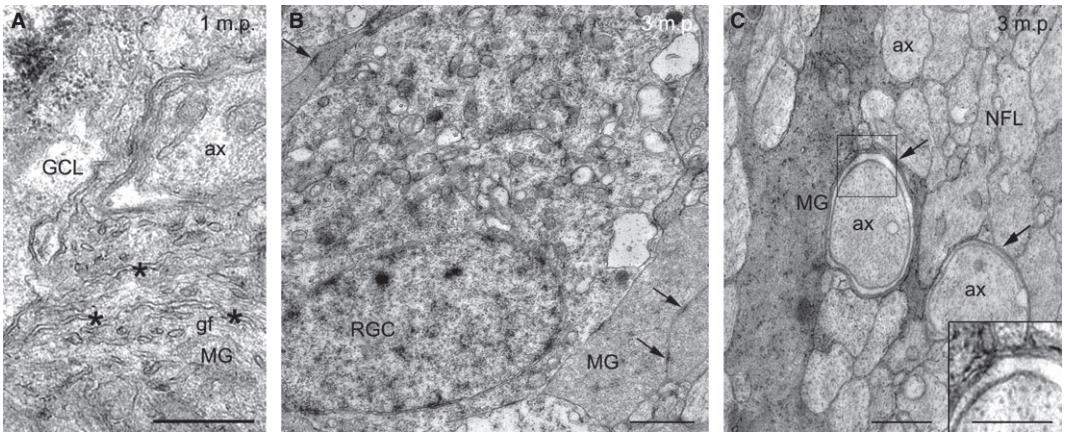

Fig. 3 Ultrastructure of Müller glia (MG) in the experimental retina. (A) Electron micrograph of the GCL at 1 m.p. Müller glia processes show developed smooth endoplasmic reticulum (asterisks) and abundant gliofilaments (gf). Note the transversally cut RGC axons (ax). (B,C) Electron micrographs in the GCL (B) and NFL (C) at 3 m.p. Electron-dense Müller glia processes are joined by desmosomes (arrows in B). Müller glia enwrap RGCs (B) and loosely myelinated axons (arrows in C). The Müller glia processes around the axons are detailed in the inset in (C). For abbreviations, see text. Scale bars: 1 μm (A-C), 0.5 μm (inset in C).

ON during different surviving post-lesion periods. A subpopulation of them was identified as GFAP$^+$ astrocytes in both nerve stumps at 3 m.p., and also in the caudal and rostral experimental nerve at later post-lesional time points (Fig. 4F).

From 6 to 12 m.p., the entire experimental optic nerve showed an apparent increase in the Vim$^+$ (Fig. 4G), GFAP$^+$ (Fig. 4H), Pax2$^+$ (Fig. 4I) and Sox9$^+$ (Fig. 4J,J′) astrocytes in comparison with that found on the contralateral intact side. Accordingly, DAPI$^+$ nuclei were clearly more numerous on the experimental side (Fig. 4J), suggesting long-term gliosis. Moreover, hypertrophied Vim$^+$ and GFAP$^+$ astrocytes delimited the borders of the decussating fascicles in the optic chiasm (Fig. 4G,H). Unlike the mild retrograde degeneration observed in the experimental optic nerve head, a marked tissue degeneration, revealed by abundant cavitation, occurred caudal to the lesion site (e.g. optic chiasm in Fig. 4G,L,M) in coexistence with the putative regrowing nerve bundles identified by anti-neurofilament immunostaining (Fig. 4I) and Nomarsky optics (arrowheads in Fig. 4M). From 1 m.p. onwards, both the Vim$^+$/CD44$^+$ astrocytes and CD44$^+$ punctate staining were observed in the experimental caudal nerve and chiasm (Fig. 4K,L).

Ultrastructural data of the astrocytes along the experimental optic nerve at 0.5, 1 and 9 m.p. were in agreement with previous immunohistochemical data. Thus, the conus papillaris-optic nerve junction showed astroglial cells with heterochromatic nuclei and enlarged cytoplasm, and with abundant gliofilaments and occasional dense bodies and lipid droplets (Fig. 5A). The hypertrophied fibrous astrocytes containing abundant gliofilaments, dilated cisternae of rough endoplasmic reticulum, lipid droplets and desmosome junctions predominated at the lesion site and also caudally, where both intact and degenerating axons were detected (Fig. 5B,C). Caudal to the lesion site, astroglial cells phagocytising myelin debris (Fig. 5C,D) were observed from neighbouring degenerated axons. At late post-lesional time points, the astrocytes accumulating lipid droplets were detected frequently in the optic chiasm (Fig. 5E) as extracellular debris decreased and large astrocyte processes filled with gliofilaments enwrapped the regenerated bundles of axons (not shown).

Immunolabelling in the experimental brain: hypothalamus, optic tract and superficial optic tectum

Proliferating periventricular cells were detected in the experimental hypothalamus (Fig. 6A–C) and optic tectum (not shown) at the different post-lesional time points of this study. A subpopulation of these PCNA$^+$ cells coexpressed Vim (not shown) and/or GFAP (Fig. 6A,B). Conversely, proliferating cells were not detected in the hypothalamus and optic tectum of the control animals (not shown). By 1 m.p. onwards, the radial glial processes in the ventral hypothalamus became intensely GFAP$^+$ (Fig. 6B) and Vim$^+$ (Fig. 6E). Moreover, the free cells expressing PCNA (Fig. 6C) and Sox9 (Fig. 6D) seemed to originate and migrate from the ventricular wall of the ventral hypothalamus by 6 m.p.

In the experimental optic tract, the Sox9$^+$ astrocytes were identified by the coexpressions of Vim (Fig. 6E), GS (Fig. 6F) and GFAP (Fig. 6G). CD44$^+$ puncta were detected in the experimental optic tract, but astrocytes persisted as CD44$^-$ (Fig. 6H), as in the control animals. Notably, Vim$^+$ astrocytes were abundantly stained in the experimental optic tract (Fig. 6H–J) but proved undetectable under control conditions (not shown) and on the contralateral side (Fig. 6J).

© 2013 Anatomical Society

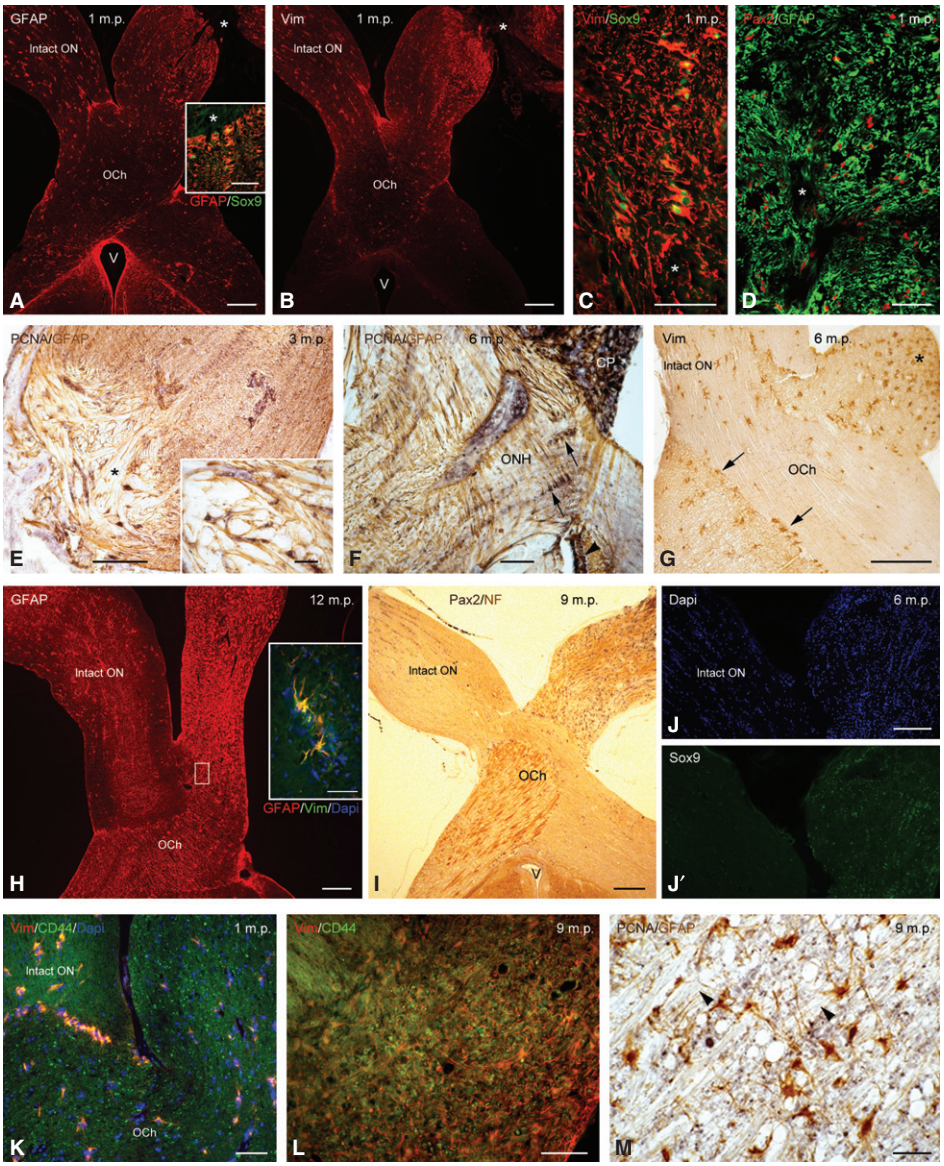

Fig. 4 Immunocharacterisation of reactive astrocytes in the experimental optic nerve and optic chiasm (OCh). Images represent horizontal sections in which rostral sides are on top. Note both immunofluorescence (A–D,H,J,J′,K,L) and the immunoperoxidase labelling using Nomarski optics (E-G, I,M). (A,B) Panoramic view of both ONs, the transection site (asterisk), OCh and the ventral hypothalamus at 1 m.p. GFAP (A) and Vim (B) staining is strong on both nerve stumps but is not detected in between (asterisk). The inset in A shows the $Sox9^+/GFAP^+$ reactive astrocytes on the caudal nerve stump, whereas the putative invasive connective tissue is unstained (asterisk). (C,D) At 1 m.p., the reactive astrocytes in the rostral nerve stump are $Vim^+/Sox9^+$ (C) and $Pax2^+/GFAP^+$ (D). Note that the putative invasive connective tissue is not stained (asterisk in C and D). (E,F) Double staining of PCNA (in black) and GFAP (in brown) on the rostral nerve stump at 3 months (E) and in the ONH at 6 months (F). Note the $GFAP^+/PCNA^+$ reactive astrocytes on the rostral nerve stump (E, details in inset) and in the experimental ONH (arrows in F). The unstained tissue in E (asterisk) and in the inset in E represent putative invasive connective tissue. Note the black pigments in the CP and the retinal pigment epithelium (arrowhead in F). (G) At 6 months, Vim^+ astrogliosis and tissue disorganisation are evident in the ON caudal to the lesion site (asterisk), and limit the decussating experimental and intact fascicles in the OCh (arrows). (H) Note the up-regulation of GFAP in the experimental ON and OCh at 12 m.p. The boxed area is detailed in the inset in H, which shows the $GFAP^+/Vim^+/Dapi^+$ reactive astrocytes limiting decussating fascicles in OCh. (I) Panoramic view of both the ONs and OCh at 9 m.p. Abundant $Pax2^+$ astrocyte nuclei (in black) and regrowing fibres intensely NF^+ (in brown) are detected on the experimental side. (J,J′) Experimental and contralateral ON at 6 m.p. $DAPI^+$ nuclei (J) and $Sox9^+$ astrocytes (J′) are apparently more abundant in the experimental ON. (K,L) Double staining for Vim and CD44 in both the ONs and OCh at 1 month (K) and in the experimental OCh at 9 months (L). $Vim^+/CD44^+$ astrocytes are observed on both the intact and experimental sides, whereas $CD44^+$ puncta are detected only in the experimental ON (K) and OCh (L). The latter show tissue cavitations surrounded by Vim^+ processes (L). (M) PCNA (in black) and GFAP (in brown) labelling the OCh at 9 m.p. $PCNA^-/GFAP^+$ astrocytes are shown among abundant tissue cavities and putative bundles of regrowing axons (arrowheads). V: ventricle. For other abbreviations, see text. Scale bars: 200 μm (A,B,E,G-J); 50 μm (inset in A,C,D, inset in E,F, inset in H,K–M).

© 2013 Anatomical Society

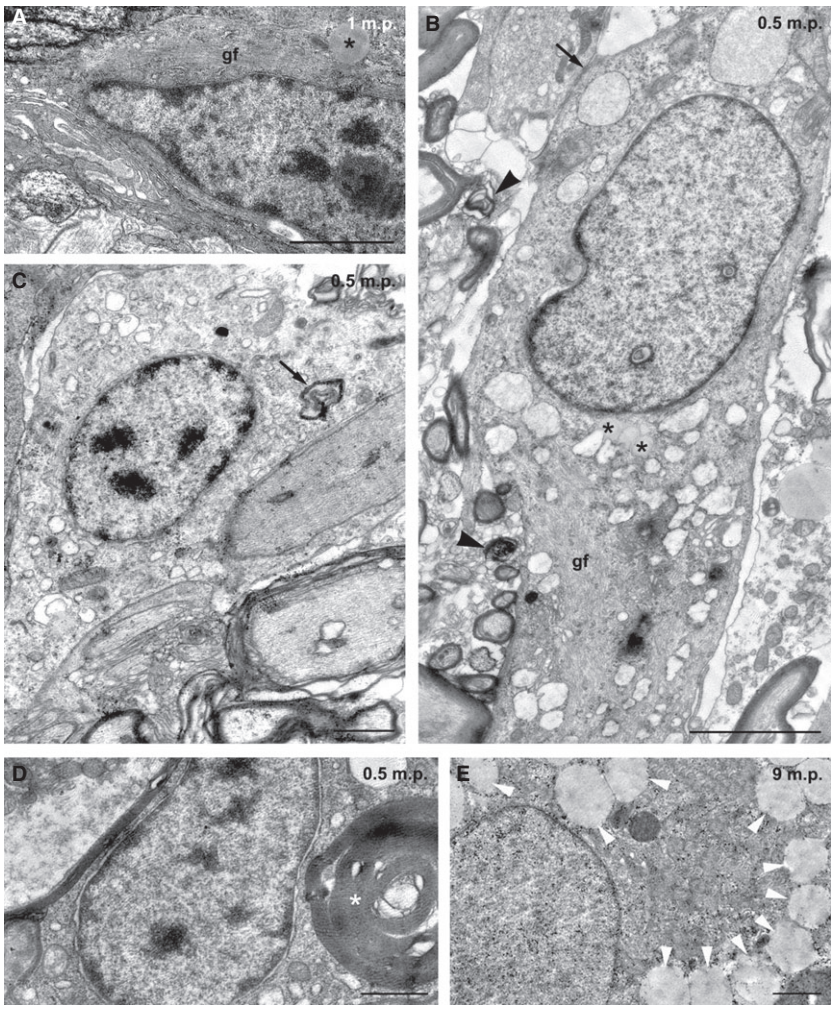

Fig. 5 Ultrastructure of the reactive astrocytes in the experimental optic nerve and optic chiasm. (A,B) Reactive fibrous astrocytes containing developed RER with dilated cisternae, abundant bundles of gliofilaments (gf) and some lipid droplets (asterisks) at the conus papillaris-optic nerve junction (A) and at the lesion site (B) at 1 and 0.5 m.p., respectively. Note the desmosome junctions between the astrocytes (arrow in B) and myelinated axons undergoing degeneration (arrowheads in B). (C,D) Caudal to the lesion site, we can see the reactive astrocytes phagocyte myelin debris (arrow in C; asterisk in D) from the degenerating axons at 0.5 m.p. (E) Ultrastructure of an astrocyte containing numerous lipid droplets (arrowheads) in the regenerating optic chiasm at 9 m.p. For abbreviations, see the text. Scale bars: 1 μm.

The abundant cystic cavities enwrapped by Vim^+ processes were persistently observed in the regenerating optic tract (Fig. 6I). The statistical analysis performed in the experimental optic tract revealed that Vim labelling significantly increased at 1 and 12 m.p., whereas that of GFAP was significant only at 12 m.p. (Fig. 1). Accordingly, the labelling of Vim and GFAP was clearly more abundant in the experimental optic tract than on the contralateral side at 12 m.p. (Fig. 6J,K).

In the experimental optic tectum, the radial glia processes enwrapped putative bundles of regenerated axons from 6 m.p. onwards (Fig. 6L). Moreover, scarce $PCNA^+$ cells were observed in the superficial optic tectum (Fig 6L), unlike the homogeneous $GFAP^+/PCNA^-$ staining of astrocytes and radial glia in the control animals (not shown). The Sox9 labelling pattern in the experimental optic tectum was apparently similar to that in the control animals, whereas the $CD44^+$ punctate labelling, as previously described in the experimental optic nerve and optic tract, was also observed in the superficial tectum (not shown).

Discussion

The limited glial response in the experimental retina may reflect functional viability

After axotomy, Müller glia underwent restricted intensification of Vim and GFAP labelling in their endfeet and inner branches. However, these changes were not statistically significant. This mild glial response correlated with limited retrograde degeneration and robust RGCs' capacity to survive (Santos, 2008; Yanes et al. 2011). The latter was demonstrated by a persistent up-regulation of the early gene c-jun, and the neuron-specific markers beta-III tubulin and HuCD (Lang et al. 2002; Romero-Alemán et al. 2010). Müller glia showed a marked development of the endoplasmic reticulum (Fig. 3A), probably involved, among other functions, in the maintenance of loose myelin sheaths in the nerve fibre layer (Fig. 3C in this study; Santos et al. 2006) and in the enlargement of inner processes which appear to protect RGCs. The absence of proliferating cells in both the control and experimental

© 2013 Anatomical Society

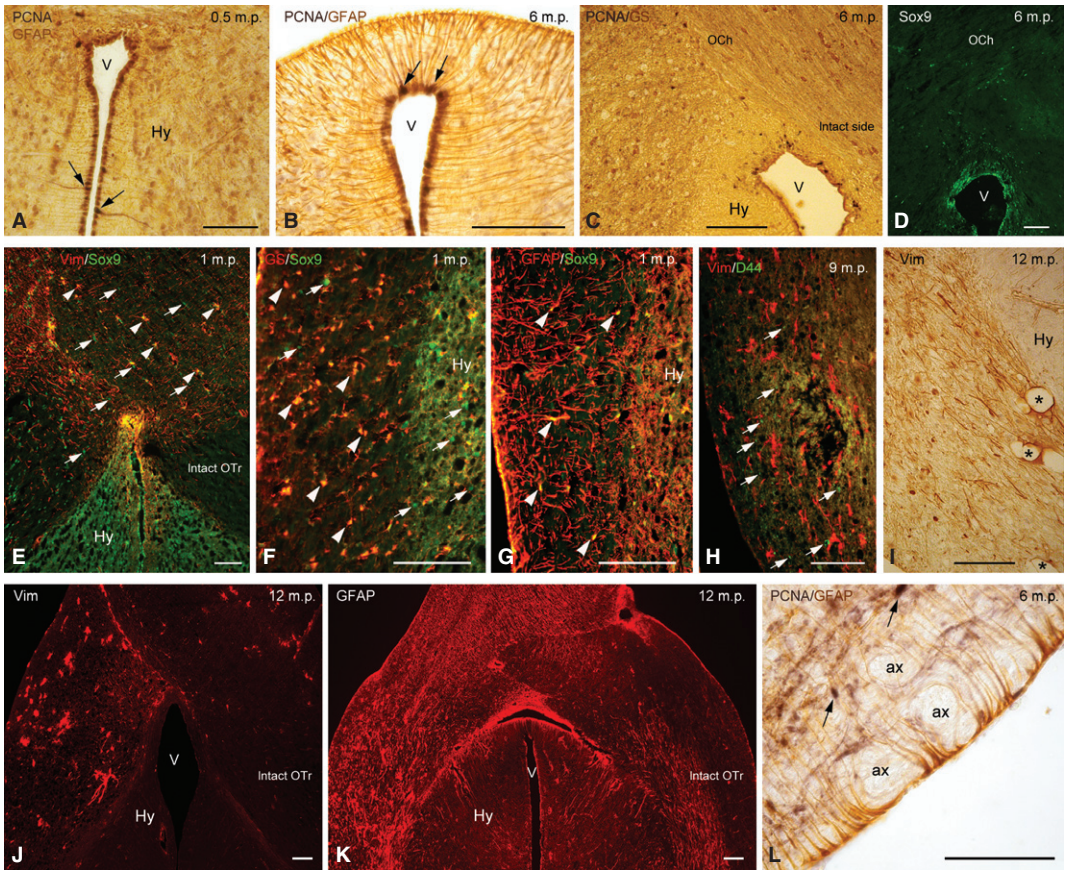

Fig. 6 Immunocharacterisation of the reactive radial glia and astrocytes in the hypothalamus (Hy; A-E), optic tract (F–K) and optic tectum (L). Images represent horizontal sections in which the rostral sides are on top. Note both the immunoperoxidase (A–C,I,L) and immunofluorescence staining (D–H,J,K). (A,B) Double labelling for PCNA (black signal) and GFAP (brown signal) in the ventral hypothalamus at 0.5 (A) and 6 m (B). Note a subpopulation of $PCNA^+/GFAP^+$ radial glia (arrows) and strong $GFAP^+$ radial glia processes at 6 months (B). (C,D) Double staining of PCNA (in black) and GS (in brown) (C) and the single labelling of Sox9 (D) at 6 m.p. $PCNA^+/GS^-$ (C) and $Sox9^+$ free cells (D) seem to migrate from the ventricular wall of the ventral hypothalamus. (E) At 1 month, note the intense $Vim^+/Sox9^+$ radial glia in the ventral hypothalamus. $Vim^+/Sox9^+$ reactive astrocytes (arrowheads) and $Vim^-/Sox9^+$ cells (arrows) are also observed in the OCh. (F,G) The double immunofluorescence for GS/Sox9 (F) and GFAP/Sox9 (G) in the experimental OTr at 1 m.p. An abundant coexpression of Sox9 and both GS and GFAP (arrowheads) is observed. $Sox9^+/GS^-$ cells (arrows in F) are also shown. (H) The double staining of Vim/CD44 in the experimental OTr at 9 m.p. Reactive astrocytes are $Vim^+/CD44^-$ and scattered $CD44^+$ puncta (arrows) are detected. (I) Vim labelling in the experimental OTr at 12 m shows the reactive astrocytes and processes enwrapping cystic cavities (asterisks). (J, K) At 12 months, the experimental OTr shows more abundant Vim^+ (J) and $GFAP^+$ (K) astrocytes than the contralateral side. (L) $GFAP^+$ radial glia processes and endfeet enwrap bundles of putative regenerated axons (ax), which are transversally cut in the superficial OT at 6 m.p. Note a few scattered $PCNA^+$ cells (arrows). For abbreviations, see text. Scale bars: 100 μm.

G. galloti retina (Lang et al. 2002; present study) agrees with the data reported for the lizard *C. ornatus* (Beazley et al. 1998) and further reinforces the reptilian model's peculiarity of true axonal regeneration when compared with that in anamniote vertebrates (see below). In addition, the apparent unchanged GS staining pattern in the experimental lizard retina (Romero-Alemán et al. 2010) very likely reflects the maintenance of Müller glia glutamate uptake and detoxification (astrocytes are not detected in the avascular lizard retina), suggesting retina viability. The high survival rate of RGCs by 12 m.p. (Santos, 2008) and the significant recovery of pupillary light reflex by 6 m.p. (Yanes et al. 2011) support this view. The glial response in the regenerating lizard retina resembled that in fish more than in mammals (see Table 2), except for some proliferation in the fish retina (McCurley & Callard, 2010), which is probably linked to its continuous neurogenesis (Lillo et al. 2002). Conversely, after optic nerve injury in regeneration-deficient amniotes such as mouse and rat, the experimental retina underwent an intense proliferation of microglia, astrocytes and Müller glia, as well as the upregulation of GFAP, Vim and nestin (Chen & Weber, 2002; Ohlsson et al. 2004; Panagis et al. 2005; Wohl et al. 2009, 2011). Taken together, the limited glial response in the retina may be linked to RGC survival and can be considered an indicator of the retinal viability after optic nerve lesion. In contrast, acute retinal injury can induce the proliferation of microglia and Müller cells in fish, chick (Stanke et al.

© 2013 Anatomical Society

Table 2 Differences among adult vertebrate visual system in control and experimental conditions.

	Amniotes			Anamniotes
	Rodent[a]	Bird[b]	Lizard[c]	Fish[d]
Retinal growth and proliferation[1,2]	Prenatal/before eye opening in amniotes			Lifelong
RGC survival after ONI[1]	<10%	ND	65–70%	90%
Retinal response after ONI[3–9,25]				
Prolif	+ (μgl, MG, As)	+ (μgl)	−	±
GFAP	+ (MG, As)	ND	+ (MG)	+ (MG)
Vim	+ (μgl, MG, As)	ND	+ (MG)	ND
Nestin	+ (μgl, MG, As)	ND	ND	ND
GS	Translocation (MG)	ND	Unchanged (MG)	ND
Immunocharacterization of astrocytes in control ON[10–21]				
Prolif	−	−	−	−
GFAP	+	+	++	+
Vim	+	+	+	+
Nestin	+	ND	ND	ND
CK	−	−	−	++
CD44	+	ND	+	ND
Pax2	+	+	+	+
Sox9	+	+	+	ND
GS	ND	ND	++	+ or − (zebrafish)
S100	+	−	+	+
Inmunocharacterization of astrogliosis after ONI[8,10,20,21,22–25]				
Prolif	+	ND	+	+
GFAP	+++	ND	+++	+ or − (zebrafish)
Vim	++	ND	++	++
Nestin	ND	ND	ND	ND
CK	−	ND	−	++
CD44	ND	ND	+	ND
Pax2	ND	ND	++	ND
Sox9	ND	ND	++	ND
GS	ND	ND	++	ND
S100	+	ND	ND	+
Astrocyte junctions in control ON[16,19,20,26]	Gap junctions in all vertebrates Desmosomes in lizard and anamniotes Tight junctions in anamniotes			
RGC axons reach the OT/SC after ONI[1,23, 27]	Failure in rodent and bird Lizard: By 1 mp (ONC); By 6–9 mp (ONT)			By 1 mp (ONC)
Cytoarchitecture of the experimental ON[1,8, 20,27]	Unrecoverable in rodent and bird Partial recovery in lizard			Resemble normal by 2 m

References

[1a–d]Berry et al. (2008); [2a–d]Farah (2006); [3a]Panagis et al. (2005); [4a]Ohlsson et al. (2004); [5a]Chen & Weber (2002); [6a]Wohl et al. (2009, 2011); [7b]Jeon et al. (2004); [8c]Present study; [9d]McCurley & Callard (2010); [10a]Nitzan et al. (2006); [11a,b]Stanke et al. (2010); [12a,b]Fischer et al. (2010); [13a]Ries et al. (2007); [14a]Frisén et al. (1995); [15c]Romero-Alemán et al. (2003, 2010); [16c]Casañas et al. (2011); [17d]Parrilla et al. (2009); [18d]Lillo et al. (2002); [19d]Grupp et al. (2010); [20d]Nona (2005); [21d]Velasco et al. (1997); [22a]Frank & Wolburg (1996); [23c]Lang et al. (2002); [24d]Cohen et al. (1994); [25d]Koke et al. (2010); [26a]Orthmann-Murphy et al. (2008); [27c]Dunlop et al. (2004)

The changes in immunolabellings are represented in an arbitrary scale from not detected (–) to very abundant (+++) followed by the staining location between brackets.

[a]Mouse; [a]Rat. [b]Chick; [b]Quail. [c]*G. galloti;* [c]*C. ornatus.* [d]Zebrafish; [d]Goldfish; [d]Tench.

As, astroglia; CK, cytokeratin; INL, inner nuclear layer; mp, month(s) post-lesion; MG, Müller glia; μgl, microglia; ND, no data; ON, optic nerve; ONC; optic nerve crush; ONI, optic nerve injury; ONT; optic nerve transection; OT, optic tectum; Prolif, proliferating cells; RGC, retinal ganglion cell; SC, superior colliculus.

© 2013 Anatomical Society

2010) and *G. galloti* (Romero-Alemán et al. unpublished data).

Reactive astrocytes and radial glia provide a structural scaffold supporting axonal regrowth

After lizard optic nerve transection, reactive astrocytes proliferated, were hypertrophied and showed abundant gliofilaments on both nerve stumps. This is in accordance with their initial beneficial function in wound closure and with the restoration of the blood–brain barrier in rodents (review in Robel et al. 2011). Our data suggest that the $GFAP^{-}/Vim^{-}/Sox9^{-}/Pax2^{-}$ cells located between both nerve stumps (asterisk in Fig. 4A–E) may correspond to invasive connective tissue (Lang et al. 1998) and/or to dedifferentiated astrocytes which have transitorily lost gliofilaments to undergo proliferation, as described in mammals (Frank & Wolburg, 1996; Nitzan et al. 2006) and fish (Nona, 2005). Additionally, the abundant $PCNA^{+}$ cells at the lesion site were identified as tomato $lectin^{+}$ macrophages/microglia (Romero-Alemán, unpublished data). An initial increase in the gliofilaments in reactive astrocytes may help their migration towards the lesion site to repair the wound, as suggested by the evidence that the reactive astrocytes from $Vim^{-/-}$ /$GFAP^{-/-}$ knockout mice require more time to close the wound defect than those from wild-type animals (Pekny et al. 1999). Moreover, these gliofilaments are essential for the intracellular transport of vesicles containing neuropeptides and growth factors (Parpura et al. 1994; Potokar et al. 2007). In fact, the axotomy triggers an abundant neurotrophin-3 expression in the astrocytes surrounding the lesion site, which may participate in the survival and subsequent regeneration of RGCs (Santos et al. 2008), such as rat optic nerve astrocytes, which secrete the ciliary neurotrophic factor to allow axonal regeneration despite glial scar formation (Berry et al. 2008).

In *G. galloti*, the lesion site became gradually colonised by reactive astrocytes, which extended caudally along the entire experimental side and persisted at late post-lesional time points in coexistence with regrowing RGC axons. Reactive astrocytes increased Vim and GFAP, and expressed Pax2 (only in the optic nerve and chiasm) and Sox9 along the experimental side. The sequential up-regulation of these intermediate filaments is reminiscent of the astrocyte differentiation process during development, since the expression of Vim also preceded that of GFAP (Monzón-Mayor et al. 1990a; Casañas et al. 2011).

Reactive radial glia in the optic tract and optic tectum showed a similar immunocharacterisation. Reactive $Pax2^{+}$ astroglia may help the packing and regrowth of RGC axons, as described in other species (see the review in Ziman et al. 2001). Moreover, permissive endfeet of Müller glia and brain radial glia are likely to rule the regrowth of lizard RGC axons, as reported during chick and rat development (Stier & Schlosshauer, 1999). In addition, rows of hypertrophied Vim^{+} astrocytes might be involved in guiding decussating fibre bundles in the optic chiasm (Fig. 4G) and in maintaining axonal integrity. The latter is suggested by the ultrastructural observation of a close relationship between regenerating axons and astrocytes (Fig. 5B). We hypothesise that Müller glia processes, reactive astrocytes and radial glia form a structural scaffold that supports axonal regrowth in the regenerating lizard visual system. Astrocyte desmosome junctions, which probably bind Vim gliofilaments, may reinforce this scaffold. Similarly, in the regenerating optic nerve of anamniotes, reactive astroglia up-regulated mainly Vim and cytokeratin (Stafford et al. 1990; Cohen et al. 1994; Koke et al. 2010), which are linked to astrocyte desmosome junctions (Rungger-Brändle et al. 1989; Maggs & Scholes, 1990). In this context, different glial junctions reflect several distinct physiological functions which may account for axonal regeneration success. Accordingly, the presence of tight junctions between glial cells in several regeneration competent systems [e.g. in astrocytes from the fish optic nerve, in astrocytes from the caudal spinal cord of the lizard *Anolis Carolinensis*, in the olfactory ensheathing glia of mammals, in Schwann cells from the peripheral nervous system (PNS) of mammals] are proposed to create micro-compartmentalisation, which is of benefit for axonal growth (Mack & Wolburg, 2006). These data raise the question of whether the absence of desmosome and tight junctions in mammalian astrocytes is balanced by a more rigid glial scar for mechanical stabilisation but which impairs nerve regeneration. Long-term glial scar in mammals has been considered largely inhibitory for axon regrowth, as it is a physical and molecular barrier due to the synthesis and secretion of inhibitory molecules, such as the CSPG (Becker & Becker, 2002; Nitzan et al. 2006). In line with this, studies into GFAP and Vim mutant mice, which exhibit reduced reactive gliosis and higher levels of regeneration, have concluded that these gliofilaments prevent regrowth after injury (Pekny et al. 1999). Nevertheless, reduced vascularisation and abnormal optic nerve myelination in $GFAP^{-/-}$ knockout mice suggest a role of GFAP in the long-term maintenance of myelination and vascularisation *in vivo* (Liedtke et al. 1996).

Reactive astrocytes remain functional, increase the secretory protein load and contribute to debris removal

It has been proposed that persistent reactive astrocytes in mammals lose their normal and essential functions (Sofroniew & Vinters, 2010). However, and quite unlikely, reactive astrocytes and radial glia in the lizard optic nerve and optic tract seem to maintain their functions, as both GS and VGLUT1 labelling showed no relevant changes after optic nerve transection (Romero-Alemán et al. 2010). The ultrastructure of reactive astrocytes in lizard displayed dilated cisternae of the rough endoplasmic

© 2013 Anatomical Society

reticulum (RER) containing abundant flocculent material (Fig. 5B,C), which is suggestive of intense protein synthesis and abnormal storage. We consider that this is not the result of a technical artefact, since the ultrastructure of other cellular organelles is well preserved. It more likely is the result of physiological RER stress (Lin et al. 2008), which probably increases the secretory protein load so markedly that it leads to an imbalance between protein folding demand and the RER capacity. A similar rationale may be involved in the finding of dilated cisternae of the RER in the astrocyte lineage during lizard and mammalian CNS development (Monzón-Mayor et al. 1990b). Ultrastructural data have also revealed a marked phagocytic function of optic nerve astrocytes throughout regeneration, as previously described in the regenerating optic nerve of fish (Colavicenzo & Levine, 2000; Nona, 2005) and rat (Frank & Wolburg, 1996). Myelin bodies and lipid droplets have been commonly observed in their enlarged cytoplasm. Thus they contribute to myelin clearance, which may enhance regeneration after optic nerve injury, as suggested in fish (Nona, 2005). The abundance of lipid droplets and the decreased myelin debris in reactive astrocytes during late regenerating periods may reflect the catabolism of phagocyted myelin debris, as described in degenerating mammalian white matter (Franson, 1988) and as occurs in Schwann cells of the regenerating mammalian PNS (Goodrum et al. 1994).

The regenerating model of the lizard visual system differs from that in anamniotes and shows mammalian-like features

The regeneration process after optic nerve injury in adult fish, amphibians and reptiles is the predominant true regeneration from damaged RGCs (see Table 2). The complete restoration of the visual functions in anamniotes differs notably from the limited functional recovery in lizards (see Table 1). The functional success in the former is linked to neither the severity of optic nerve injury (i.e. crush or transection) or the differences in the anatomical complexity of the chiasm among species (Jeffery & Erskine, 2005; Mogi et al. 2009). It is more likely that the presence of adult retinal neurogenesis and the highly supportive CNS microenvironment (see below) are pivotal factors. Notably, lifelong retinal neurogenesis is lacking in the lizard species (Beazley et al. 1998; Lang et al. 2002; Dunlop et al. 2004; Casañas et al. 2011). In addition, typical axonal growth inhibitors in the mammalian CNS (e.g. tenascin-R, Nogo-A) are lacking or down-regulated during optic nerve regeneration in anamniotes (Becker et al. 1999, 2004) but are up-regulated in the regenerating *G. galloti* optic nerve and optic tract (Lang et al. 1998, 2008). Up-regulation of axonal growth promoters (e.g. laminin and fibronectin) in *G. galloti* has been suggested to override the effects of these axonal growth inhibitors (Lang et al. 2008).

In relation to the glial microenvironment, the characterisation of *G. galloti* optic nerve astrocytes ($GFAP^+$, Vim^+, $S100^+$, GS^+, $CD44^+$, $cytokeratin^-$) better resembles that in mammals than in fish (see Table 2), although astrocyte desmosome junctions are described in the optic nerve of both fish and lizard, but not in mammals. Moreover, radial glia and astrocytes coexist and show a similar immunocharacterisation in the adult midbrain of *G. galloti* (Monzón-Mayor et al. 1990a), whereas only radial glia are described in the brain of anamniotes, and only astrocytes in the brain of regeneration-deficient amniotes, birds and mammals (Robel et al. 2011). Thus, persisting radial glia in adult lizard (Monzón-Mayor et al. 1990a,c) and fish may provide permissive substrates for axonal regeneration and neurogenic potential in the brain (Romero-Alemán et al. 2010; Robel et al. 2011). In addition, gliosis in the regenerating goldfish optic nerve is transitory (Stafford et al. 1990), whereas invading Schwann cells promote axon regrowth and remyelination (Nona et al. 2000), and restoration of the tissue cytoarchitecture is accomplished by 3 m.p. (Nona, 2005). In contrast, gliosis in the regenerating lizard optic nerve and optic tract is persistent and regrowing fibres coexist with myelin debris (Lang et al. 2008; Santos, 2008) and abundant cystic cavities (Figs 4L,M and 6C,I), which are not detected in fish and constitute impenetrable obstacles for growing axons in rat CNS (Dusart & Sotelo, 1994). Taken together, the lizard model might prove useful to understand the molecular mechanisms of the marked loss of regeneration competence in mammals.

Conclusions

We conclude that long-term astrogliosis, persistent tissue disorganisation and successful axonal regrowth coexist in the lizard visual system. Reactive astrocytes and radial glia are strongly $GFAP^+$ and Vim^+, forming a structural scaffold that supports axonal regeneration. Abundant Sox9 and Pax2 labelling reflects an increased reactive astroglial population, which also contributes to debris removal, increases the secretory protein load, and maintains the glutamate-glutamine cycle along the regenerating optic pathway.

Acknowledgements

This study was supported by the Spanish Ministry of Education [grant number BFU2007-67139] and by the Canary Islands Regional Government [grant number SolSubC200801000281; grant number ULPAPD-08/01-4] to M.M.M. The authors are grateful to Prof. Dr Pedro Saavedra (Dept. of Mathematics, ULPGC) for his support in the statistical analysis. Sara Diepa and Nieves Casañas are also acknowledged for their excellent technical assistance. The collaboration of the Electron Microscopy Services of the University of de Las Palmas de Gran Canaria (ULPGC) and the Universty of de La Laguna (ULL) is also appreciated. The

© 2013 Anatomical Society

H5 monoclonal antibody was obtained from the Developmental Studies Hybridoma Bank, developed under the auspices of the NICHD and maintained by the University of Iowa, Department of Biological Sciences.

Author contributions

M.M.R.A. carried out the immunohistochemical study and contributed to the measurements, design and writing of the manuscript. M.M.M. participated in the conception, design, coordination of the study and writing of the manuscript. E.S. carried out the ultrastructural study and contributed to writing the manuscript. C.M.Y. participated in writing the manuscript and in coordinating the study. All the authors have read and approved the final manuscript.

References

Beazley LD, Sheard PW, Tennant M, et al. (1997) Optic nerve regenerates but does not restore topographic projections in the lizard *Ctenophorus ornatus*. *J Comp Neurol* **377**, 105–120.

Beazley LD, Tennant M, Stewart TM, et al. (1998) The primary visual system of adult lizards demonstrates that neurogenesis is not obligatorily linked to central nerve regeneration but may be a prerequisite for the restoration of maps in the brain. *Vision Res* **38**, 789–793.

Beazley LD, Rodger J, Chen P, et al. (2003) Training on a visual task improves the outcome of optic nerve regeneration. *J Neurotrauma* **20**, 1263–1270.

Becker CG, Becker T (2002) Repellent guidance of regenerating optic axons by chondroitin sulphate glycosaminoglycans in zebrafish. *J Neurosci* **22**, 842–853.

Becker CG, Becker T, Meyer RL, et al. (1999) Tenascin-R inhibits the growth of optic fibers *in vitro* but is rapidly eliminated during nerve regeneration in the salamander *Pleurodeles waltl*. *J Neurosci* **19**, 813–827.

Becker CG, Schweitzer J, Feldner J, et al. (2004) Tenascin-R as a repellent guidance molecule for newly growing and regenerating optic axons in adult zebrafish. *Mol Cell Neurosci* **26**, 376–389.

Benton RL, Ross CD, Miller KE (2000) Glutamine synthetase activities in spinal white and gray matter 7 days following spinal cord injury in rats. *Neurosci Lett* **291**, 1–4.

Berry M, Ahmed Z, Lorber B, et al. (2008) Regeneration of axons in the visual system. *Restor Neurol Neurosci* **26**, 147–174.

Busch SA, Silver J (2007) The role of extracellular matrix in CNS regeneration. *Curr Opin Neurobiol* **17**, 20–127.

Caminos E, Becker E, Martín-Zanca D, et al. (1999) Neurotrophins and their receptors in the tench retina during optic nerve regeneration. *J Comp Neurol* **404**, 321–331.

Casañas N, Santos E, Yanes C, et al. (2011) Development of astroglia heterogeneously expressing Pax2, vimentin and GFAP during the ontogeny of the lizard (*Gallotia galloti*) optic pathway: Immunohistochemical and ultrastructural study. *Cell Tissue Res* **345**, 295–311.

Chen H, Weber AJ (2002) Expression of glial fibrillary acidic protein and glutamine synthetase by Müller cells after optic nerve damage and intravitreal application of brain-derived neurotrophic factor. *Glia* **38**, 115–125.

Cohen I, Sivron T, Lavie V, et al. (1994) Vimentin immunoreactive glial cells in the fish optic nerve: implications for regeneration. *Glia* **10**, 16–29.

Colavicenzo J, Levine RL (2000) Myelin debris clearance during Wallerian degeneration in the goldfish visual system. *J Neurosci Res* **59**, 47–62.

Dharmarajan S, Belecky-Adams T, Sheibani N (2012) *Bmp Pathway and Retinal Astrogliosis*. Fort Lauderdale, FL: Abstracts ARVO Ann Meet.

Dobson B (2010) *Analysis of the expression pattern and functional role of Nogo-A and its receptor during optic nerve regeneration in the lizard Gallotia galloti*. Doctoral Thesis. Faculty of Health Sciences, University of Cape Town, Republic of South Africa.

Dunlop SA, Tran N, Tee LB, et al. (2000) Retinal projections throughout optic nerve regeneration in the ornate dragon lizard, *Ctenophorus ornatus*. *J Comp Neurol* **16**, 188–200.

Dunlop SA, Tee LBG, Stirling RV, et al. (2004) Failure to restore vision after optic nerve regeneration in reptiles: Interspecies variation in response to axotomy. *J Comp Neurol* **478**, 292–305.

Dunlop SA, Tee LB, Goossens MA, et al. (2007) Regenerating optic axons restore topography after incomplete optic nerve injury. *J Comp Neurol* **505**, 46–57.

Dusart I, Sotelo C (1994) Lack of Purkinje cell loss in adult rat cerebellum following protracted axotomy: Degenerative changes and regenerative attempts of the severed axons. *J Comp Neurol* **347**, 211–232.

Farah MH (2006) Neurogenesis and cell death in the ganglion cell layer of vertebrate retina. *Brain Res Rev* **52**, 264–274.

Fischer A, Zelinka C, Scott MA (2010) Heterogeneity of glia in the retina and optic nerve of birds and mammals. *PLoS ONE* **5**, e10774.

Frank M, Wolburg H (1996) Cellular reactions at the lesion site after crushing of the rat optic nerve. *Glia* **16**, 227–240.

Franson P (1988) Quantitative electron microscopic observations on the non-neuronal cells and lipid droplets in the posterior funiculus of the kitten after dorsal rhizotomy. *Anat Embryol* **178**, 95–105.

Frisén J, Johansson CB, Török C, et al. (1995) Rapid, widespread, and longlasting induction of nestin contributes to the generation of glial scar tissue after CNS injury. *J Cell Biol* **131**,453–464.

Goodrum JF, Earnhardt T, Gaines N, et al. (1994) Fate of myelin lipids during degeneration and regeneration of peripheral nerve: An autoradiographic study. *J Neurosci* **14**, 357–367.

Gris P, Tighe A, Levin D, et al. (2007) Transcriptional regulation of scar gene expression in primary astrocytes. *Glia* **55**, 1145–1155.

Grupp L, Wolburg H, Mack AF (2010) Astroglial structures in the zebrafish brain. *J Comp Neurol* **518**, 4277–4287.

Harman AM, Rodger J, Ahmat A, et al. (2003) PSA-NCAM is up-regulated during optic nerve regeneration in lizard but not in goldfish. *Exp Neurol* **182**, 180–185.

Jeffery G, Erskine L (2005) Variations in the architecture and development of the vertebrate optic chiasm. *Prog Retin Eye Res* **24**, 721–753.

Jeon GS, Kang TC, Park SW, et al. (2004) Microglial responses in the avascular quail retina following transection of the optic nerve. *Brain Res* **1023**, 15–23.

Koke JR, Mosier AL, García DM (2010) Intermediate filaments of zebrafish retinal and optic nerve astrocytes and Müller glia: differential distribution of cytokeratin and GFAP. *BMC Res Notes* **3**, 50.

© 2013 Anatomical Society

Kordes U, Hagel C (2006) Expression of Sox9 and Sox10 in central neuroepithelial tumors. *J Neurooncol* **80**, 151–155.

Laird NM, Ware JH (1982) Random-effects models for longitudinal data. *Biometrics* **38**, 963–974.

Lang DM, Monzón-Mayor M, Bandtlow CE, et al. (1998) Retinal axon regeneration in the lizard *Gallotia galloti* in the presence of CNS myelin and oligodendrocytes. *Glia* **23**, 61–74.

Lang DM, Romero-Alemán MM, Arbelo-Galván JF, et al. (2002) Regeneration of retinal axons in the lizard *Gallotia galloti* is not linked to generation of new retinal ganglion cells. *J Neurobiol* **52**, 322–335.

Lang DM, Monzón-Mayor M, Romero-Alemán MM, et al. (2008) Tenascin-R and axon growth promoting molecules are upregulated in the regenerating visual pathway of the lizard (*Gallotia galloti*). *Dev Neurobiol* **68**, 899–916.

Liedtke W, Edelmann W, Bieri PL, et al. (1996) GFAP is necessary for the integrity of CNS white matter architecture and long-term maintenance of myelination. *Neuron* **17**, 607–615.

Lillo C, Velasco A, Jimeno D, et al. (2002) The glial design of a teleost optic nerve head supporting continuous growth. *J Histochem Cytochem* **50**, 1289–1302.

Lin JH, Walter P, Yen TSB (2008) Endoplasmic reticulum stress in disease pathogenesis. *Annu Rev Pathol Mech Dis* **3**, 399–425.

Mack AF, Wolburg H (2006) Growing axons in fish optic nerve are accompanied by astrocytes interconnected by tight junctions. *Brain Res* **1103**, 25–31.

Maggs A, Scholes J (1990) Reticular astrocytes in the fish optic nerve: macroglia with epithelial characteristics form an axially repeated lacework pattern, to which nodes of Ranvier are apposed. *J Neurosci* **10**, 1600–1614.

McCurley AT, Callard GV (2010) Time course analysis of gene expression patterns in zebrafish eye during optic nerve regeneration. *J Exp Neurosci* **2010**, 17–33.

Mogi K, Misawa K, Utsunomiya K, et al. (2009) Optic chiasm in the species of order Clupeiformes, family Clupeidae: Optic chiasm of *Spratelloides gracilis* shows an opposite laterality to that of *Etrumeus teres*. *Laterality* **14**, 495–514.

Monzón-Mayor M, Yanes C, Ghandour MS, et al. (1990a) Glial fibrillary acidic protein and vimentin immunohistochemistry in the developing and adult midbrain of the lizard *Gallotia galloti*. *J Comp Neurol* **295**, 569–579.

Monzón-Mayor M, Yanes C, James JL, et al. (1990b) An ultrastructural study of the development of astrocytes in the midbrain of the lizard. *J Anat* **170**, 33–41.

Monzón-Mayor M, Yanes C, Tholey G, et al. (1990c) Immunohistochemical localization of glutamine synthetase in mesencephalon and telencephalon of the lizard *Gallotia galloti* during ontogeny. *Glia* **3**, 81–97.

Moon C, Heo S, Sim KB, et al. (2004) Upregulation of CD44 expression in the spinal cords of rats with clip compression injury. *Neurosci Lett* **367**, 133–136.

Nitzan A, Kermer P, Shirvan A, et al. (2006) Examination of cellular and molecular events associated with optic nerve axotomy. *Glia* **54**, 545–556.

Nona S (2005) Regeneration in the Goldfish Visual System (Updated 2007). In: *Webvision (internet): The Organization of the Retina and Visual System* (eds Kolb H, Fernandez E, Nelson R), pp. 1–39. Salt Lake City: University of Utah Health Sciences Center.

Nona SN, Thomlinson AM, Bartlett CA, et al. (2000) Schwann cells in the regenerating fish optic nerve: evidence that CNS axons, not the glia, determine when myelin formation begins. *J Neurocytol* **29**, 285–300.

Ohlsson M, Mattsson P, Svensson M (2004) A temporal study of axonal degeneration and glial scar formation following a standardized crush injury of the optic nerve in the adult rat. *Restor Neurol Neurosci* **22**, 1–10.

Orthmann-Murphy JL, Abrams CK, Scherer SS (2008) Gap junctions couple astrocytes and oligodendrocytes. *J Mol Neurosci* **35**, 101–116.

Panagis L, Thanos S, Fischer D, et al. (2005) Unilateral optic nerve crush induces bilateral retinal glial cell proliferation. *Eur J Neurosci* **21**, 2305–2309.

Parpura V, Basarsky TA, Liu F, et al. (1994) Glutamate-mediated astrocyte-neuron signalling. *Nature* **369**, 744–747.

Parrilla M, Lillo C, Herrero-Turrion MJ, et al. (2009) Pax2 in the optic nerve of the goldfish, a model of continuous growth. *Brain Res* **1255**, 75–88.

Pekny M, Johansson CB, Eliasson C, et al. (1999) Abnormal reaction to central nervous system injury in mice lacking glial fibrillary acidic protein and vimentin. *J Cell Biol* **145**, 503–514.

Potokar M, Kreft M, Li L, et al. (2007) Cytoskeleton and vesicle mobility in astrocytes. *Traffic* **8**, 12–20.

R Development Core Team ((2012) *R: A Language and Environment for Statistical Computing*. Vienna: R Foundation for Statistical Computing. ISBN3-900051-07-0, URL http://www.R-project.org/.

Ries A, Goldberg JL, Grimpe B (2007) A novel biological function for CD44 in axon growth of retinal ganglion cells identified by a bioinformatics approach. *J Neurochem* **103**, 1491–1505.

Rio JP, Reperant J, Ward R, et al. (1989) A preliminary description of the regeneration of optic nerve fibres in a reptile *Vipera aspis*. *Brain Res* **479**, 151–156.

Robel S, Berninger B, Götz M (2011) The stem cell potential of glia: lessons from reactive gliosis. *Nat Rev Neurosci* **12**, 88–104.

Rodger J, Bartlett CA, Harman AM, et al. (2001) Evidence that regenerating optic axons maintain long-term growth in the lizard *Ctenophorus ornatus*: growth-associated protein-43 and gefiltin expression. *Neuroscience* **102**, 647–654.

Romero-Alemán MM, Monzón-Mayor M, Yanes C, et al. (2003) S100 immunoreactive glial cells in the forebrain and midbrain of the lizard *Gallotia galloti* during ontogeny. *J Neurobiol* **57**, 54–66.

Romero-Alemán MM, Monzón-Mayor M, Yanes C, et al. (2004) Radial glial cells, proliferating periventricular cells, and microglia might contribute to successful structural repair in the cerebral cortex of the lizard *Gallotia galloti*. *Exp Neurol* **188**, 74–85.

Romero-Alemán MM, Monzón-Mayor M, Santos E, et al. (2010) Expression of neuronal markers, synaptic proteins and glutamine synthetase in the control and regenerating lizard visual system. *J Comp Neurol* **518**, 4067–4087.

Romero-Alemán MM, Monzón-Mayor M, Santos E, et al. (2012) Neuronal and glial differentiation during lizard (*Gallotia galloti*) visual system ontogeny. *J Comp Neurol* **520**, 2163–2184.

Rungger-Brändle E, Achtstätter T, Franke WW (1989) An epithelium type cytoskeleton in a glial cell: astrocytes of amphibian optic nerves contain cytokeratin filaments and are connected by desmosomes. *J Cell Biol* **109**, 705–716.

Santos E (2008) *Estudio de las neurotrofinas NT-3 y BDNF, mielinización y diferenciación macroglial durante la ontogenia y la regeneración de la vía óptica de Gallotia galloti*. Doctoral Thesis. University of La Laguna, Spain.

© 2013 Anatomical Society

Santos E, Yanes CM, Monzón-Mayor M, et al. (2006) Peculiar and typical oligodendrocytes are involved in an uneven myelination pattern during the ontogeny of the lizard visual pathway. *J Neurobiol* **66**, 1115–1124.

Santos E, Monzón-Mayor M, Romero-Alemán MM, et al. (2008) Distribution of neurotrophin-3 during the ontogeny and regeneration of the lizard (*Gallotia galloti*) visual system. *Dev Neurobiol* **68**, 31–44.

Santos E, Romero-Alemán MM, Monzón-Mayor M, et al. (2011) Expression of BDNF and NT-3 during the ontogeny and regeneration of the lacertidian (*Gallotia galloti*) visual system. *Dev Neurobiol* **71**, 836–853.

Schweitzer J, Becker T, Becker CG (2003) Expression of protein zero is increased in lesioned axon pathways in the central nervous system of adult zebrafish. *Glia* **41**, 301–317.

Sofroniew MW, Vinters HV (2010) Astrocytes: biology and pathology. *Acta Neuropathol* **119**, 7–35.

Stafford CA, Shehab SAS, Nona SN, et al. (1990) Expression of glial fibrillary acidic protein (GFAP) in goldfish optic nerve following injury. *Glia* **3**, 33–42.

Stanke J, Moose HE, El-Hodiri HM, et al. (2010) A comparative study of Pax2 expression in glial cells in the retina and optic nerve of birds and mammals. *J Comp Neurol* **518**, 2316–2333.

Stier H, Schlosshauer B (1999) Cross-species collapse activity of polarized radial glia on retinal ganglion cell axons. *Glia* **25**, 143–153.

Stolt CC, Lommes P, Sock E, et al. (2003) The Sox9 transcription factor determines glial fate in the developing spinal cord. *Genes Dev* **17**, 1677–1689.

Velasco A, Briñón JG, Caminos E, et al. (1997) S-100-positive glial cells are involved in the regeneration of the visual pathway of teleosts. *Brain Res Bull* **43**, 327–336.

Wohl SG, Schmeer CW, Kretz A, et al. (2009) Optic nerve lesion increases cell proliferation and nestin expression in the adult mouse eye *in vivo*. *Exp Neurol* **219**, 175–186.

Wohl SG, Schmeer CW, Friese T, et al. (2011) *In situ* dividing and phagocytosing retinal microglia express nestin, vimentin, and NG2 *in vivo*. *PLoS ONE* **6**, e22408.

Yanes C, Santos E, Romero-Alemán MM, et al. (2011) Recovery of pupillary light reflex but not of behavioural responses occurs after complete optic nerve transection in the lizard *Gallotia galloti*. *Glia* **59**(Suppl 1), S95–S95.

Ziman MR, Rodger J, Chen P, et al. (2001) Pax genes in development and maturation of the vertebrate visual system: implications for optic nerve regeneration. *Histol Histopathol* **16**,239–249.

© 2013 Anatomical Society